NDT&E International 84 (2016) 47–53

Contents lists available at ScienceDirect

NDT&E International

journal homepage: www.elsevier.com/locate/ndteint

Non-destructive and non-contacting stress–strain characterization of aerospace metallic alloys using photo-thermo-mechanical radiometry

Huiting Huan [a,b], Andreas Mandelis [a,b,*], Lixian Liu [a,b], Alexander Melnikov [b]

[a] School of Optoelectronic Information, University of Electronic Science and Technology of China, Chengdu 610054, China
[b] Center for Advanced Diffusion-Wave and Photoacoustic Technologies (CADIPT), Department of Mechanical and Industrial Engineering, University of Toronto, Toronto, ON, Canada M5S 3G8

ARTICLE INFO

Article history:
Received 20 May 2016
Received in revised form
14 July 2016
Accepted 22 July 2016
Available online 30 July 2016

Keywords:
Aerospace metal components
Non-contact
Non-destructive
Photo-thermo-mechanical radiometry
Stress–strain relation

ABSTRACT

A photo-thermo-mechanical non-destructive inspection methodology was developed theoretically and experimentally for non-contact, non-destructive evaluation of mechanical stress–strain relations in metallic materials. A one-dimensional thermal-wave model modified to include mechanical stress explicitly was used to fit experimental data from both frequency scan and stress scan tests and determine the thermal effusivity and diffusivity of an aerospace-industry-relevant aluminum 6061 alloy. Within the elastic regime the thermal conductivity values measured from both photothermal radiometry (PTR) amplitude and phase showed very good agreement, thereby establishing the self-consistency of the new photo-thermo-mechanical radiometry (PTMR) method. Furthermore, a linear conductivity–stress dependence was found, thus establishing the dominant role this property plays in the ability of PTMR to monitor mechanical changes in the aluminum alloy. It was demonstrated that PTMR can be used as a non-contact "strain gauge" within and far beyond the operational strain range of commercial strain gauges, up to the fracture point.

1. Introduction

In the field of non-destructive testing (NDT), the mechanical strength of metallic materials is always regarded as an important issue. Fatigue resulting from overloading or multiple cyclic loading underlies the final failure of mechanical structures or facilities. Many investigations have been reported on measuring the strength of elastic materials using NDT methodologies. Most popular techniques used include ultrasound [1,2], Raman spectroscopy [3] and X-ray diffraction [4]. Landau et al. [5] established the theoretical basis for thermal effects and elasticity, which implies anisotropic thermal property changes due to stress. The elastic property dependence on external loading has also been discussed theoretically by Biot [6] and experimentally investigated by Hughes et al. [7] The phenomenon is generally referred to as acoustoelasticity [8]. Wong et al. [9] theoretically explored the application of stress pattern analysis by the thermal emission (SPATE) technique and connected Young's modulus with the stress–strain state of metals, which establishes a theoretical basis for further experimental investigations [10]. Muratikov et al. [11,12] used a photoacoustic approach to detect residual stress in metals within the framework of non-linear thermoelastic theory. However, most of these investigations were designed for residual stress or fatigue diagnosis in damaged samples which have already become plastically deformed and are unstable. These methodologies also require a contacting transducer (e.g. PZT) for specific acoustic signal detection. Furthermore, the inspection uses large and complicated apparatus for the analysis. Regardless of the approach, those earlier methodologies did not aim at early-stage stress–strain material characterization or quantification of that relation, nor did they target system development for industrial applications use.

Unlike the conventional photoacoustic (or laser ultrasonic) approach which is closely related to both thermal and elastic properties of a material but requires a fluid couplant or direct contact between sample and transducer, this work reports an application of frequency domain photothermal radiometry (PTR) to the mechanical strength quantification of metallic industrial alloys. The methodology is based on photo-thermo-mechanical (PTM) effects which are more straightforward and easier to interpret than ultrasonic wave processes (including mode conversions). It involves only the thermal parameter dependence on stress and is not sensitive to surface deformation [13]. From the practical point of view, photo-thermo-mechanical radiometry (PTMR) eliminates the need for a coupling medium, thereby

* Corresponding author at: Center for Advanced Diffusion-Wave and Photoacoustic Technologies (CADIPT), Department of Mechanical and Industrial Engineering, University of Toronto, Toronto, ON, Canada M5S 3G8.
E-mail address: mandelis@mie.utoronto.ca (A. Mandelis).

http://dx.doi.org/10.1016/j.ndteint.2016.07.005
0963-8695/

emerging as a truly non-contacting mechanical-property measuring NDT methodology. The testing system was designed for flexibility and non-contact operation by use of a fiber-coupled laser and a mid-infrared detector. A specially designed dynamic tensile rig enabled full tensile range tests from the stress-free state up to fracture. Testing of the mechanical system consisted of two parts: a) the reversibility and reproducibility of the PTMR signal was verified by applying several rounds of cyclic tensile load on the sample within the elastic regime; and b) the sample was subsequently loaded and stressed up to fracture. The full strain-signal history of the sample was interpreted within the conventional stress–strain relation framework, thereby validating PTMR as a non-contact "strain gauge" capable of measuring this mechanical property for values of strain well beyond commercial strain gauges and up to the point of material fracture. The significance of the greatly extended dynamic range of the PTMR strain gauge is that it can keep track of the inspected material's mechanical properties and their small (early) changes, thereby monitoring the onset and evolution of fatigue cracks and other loading-related defects throughout the component's service lifetime from the original unloaded state to fracture.

2. Photo-thermo-mechanical instrumentation

A non-destructive testing apparatus consisting of both force application module and the stress/defect detection module was designed and implemented, Fig. 1. The apparatus mainly consisted of two major components, namely the tensile tester and the PTR set-up [14]. The tensile tester can apply a tensile force to elongate a metallic specimen within the elastic range and provides control for reliable and reproducible correlation between the applied specimen strain and the PTR amplitude and phase of the detected laser signal [14]. As shown in Fig. 2, a sample was made of aluminum 6061, a kind of alloy widely used in the aerospace industry. The metal was machined into a "dog-bone" shape to concentrate the stress in the middle part. An adhesive strain gauge was affixed on the back surface as a means of quantitative reference strain. An 808 nm laser (4 W peak power, beam spotsize: 7 mm in diameter) was used as a photothermal source modulated in a low frequency range (1–30 Hz). The infrared thermal radiation was collected and focused on a mercury-cadmium-telluride (MCT) detector. The output signal was processed through a lock-in amplifier and digitized in terms of amplitude and phase.

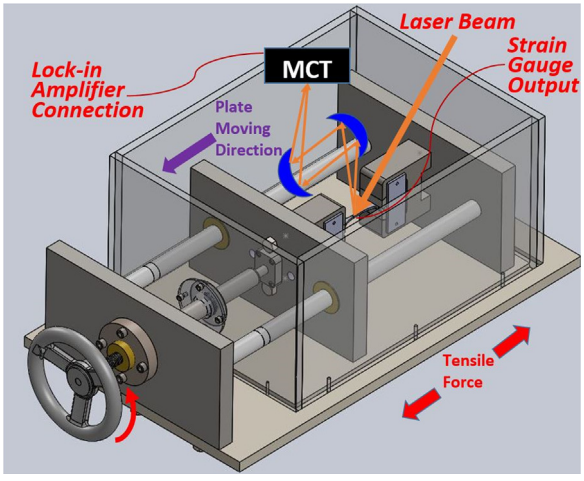

Fig. 1. Tensile tester and visual guide to its operation.

Tensile stress was applied through the axial motion holder and a stationary holder onto which the sample was pinned as shown in Fig. 1. All the tests were conducted after the sample reached mechanical equilibrium. With the strain gauge readings as a reference, the first set of experiments was focused on performing multiple cyclic loadings of the sample within the elastic regime. The frequency was scanned from 1 to 30 Hz and signal-vs-frequency data were recorded at various strain values. To maximize sensitivity, some groups of cyclic tests were conducted with higher strain resolution and smaller strain increments at a single frequency. During the second set of experiments the sample was stressed until fracture and the PTR signal from the entire stressing history was displayed.

3. Photo-thermo-mechanical radiometry (PTMR) theory

3.1. Finite element analysis (FEA) of tensile stress

For a homogeneous, isotropic material, the linear constitutive relation follows the basic Hooke's law [15]:

$$\boldsymbol{\tau} = \mathbf{C}: \boldsymbol{\varepsilon} \tag{1}$$

$\boldsymbol{\tau}$, $\boldsymbol{\varepsilon}$ are, respectively, the stress and strain tensor of order two; $\mathbf{C}$ is the elastic modulus tensor of order four. For any external load vector $\mathbf{F}$, the balance of forces requires:

$$\nabla\cdot\boldsymbol{\tau} = -\mathbf{F} \tag{2}$$

In most cases, there is no analytical solution to Eq. (2), especially for complex sample geometries. FEA is a useful engineering computational approach to determine the stress components of the sample under external load. In this work, the purpose of FEA was to determine the elastic regime range within which the reproducibility and reversibility of the system has been studied and verified. A 3-D model was created with COMSOL Multiphysics®, Solid Mechanics Module. The boundary conditions are noted in Fig. 3(a). The constraints were all applied on the lateral surface of two holes, to simulate the behavior of the pins, the motion holder and the stationary holder. The stress–strain relation of the central part is depicted in Fig. 3(b), the result of considering only elastic deformation. Given that the yield strength for aluminum 6061 T-6 is above 240 MPa [16], the strain should be far below 0.0035 to ensure the sample is within the elastic regime.

3.2. Heat conduction equation for a solid under stress

As discussed in Refs. [5,11], the existence of an external load will result in anisotropic properties in elastic bodies. The generalized form of the thermal diffusion equation in an anisotropic body is:

$$\rho C\frac{\partial T}{\partial t} - \nabla\cdot\left(\mathbf{k}\cdot\nabla T\right) = g \tag{3}$$

ρ, C are the density and specific heat capacity of the solid, respectively, g is the heat source, and $\mathbf{k} = k_{ij}(\boldsymbol{\tau})$, $i, j = x_1, x_2, x_3$ is the stress dependent thermal conductivity tensor which is symmetric, i.e. $k_{ij} = k_{ji}$. All the differentiation operations in Eq. (3) are with respect to the undeformed state, represented by the coordinates (x_1, x_2, x_3). However, the PTMR signal is collected at every equilibrium state of deformation and is thus labeled with a deformed body coordinates (X_1, X_2, X_3). The relation between the two coordinate systems is [6,17]:

$$X_i = x_i + u_i,\ i = 1, 2, 3 \tag{4}$$

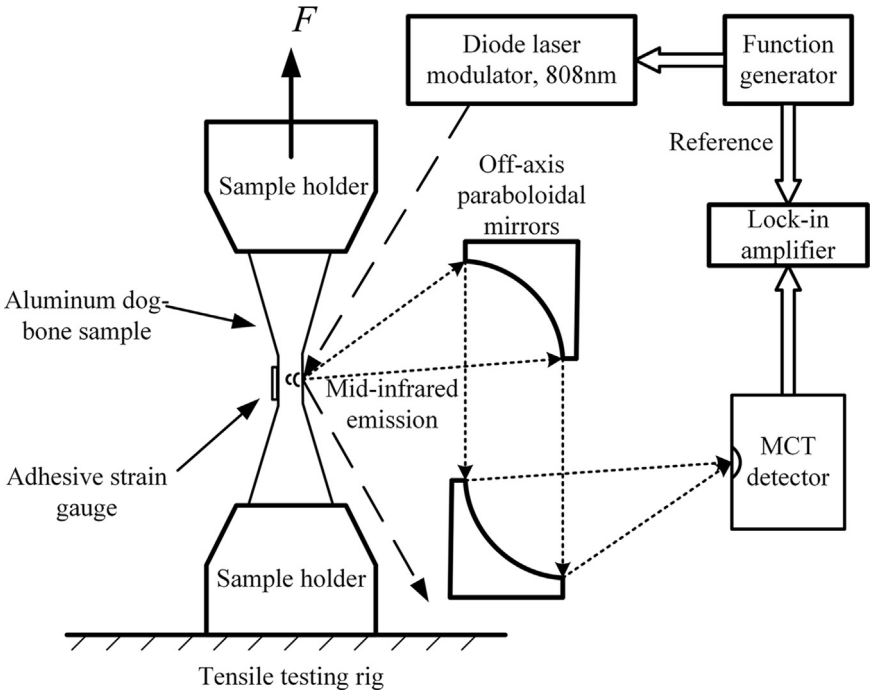

Fig. 2. Experimental schematic of photo-thermo-mechanical measurements.

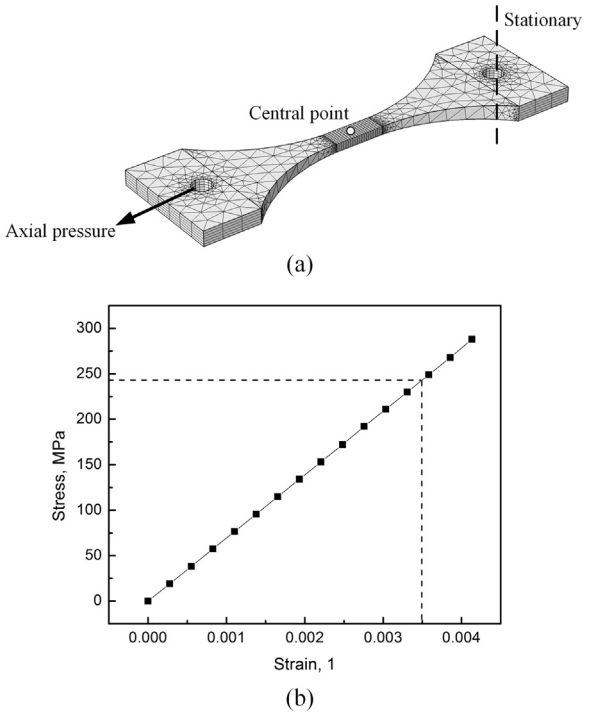

Fig. 3. (a) FEA model and (b) simulated stress–strain relation at the center.

u_i is the displacement component along the x_i axis. For simplification, the subscript summation convention is used where repeated subscripts denote a sum over sequential indexes $i, j, l, m = 1, 2, 3$ and a comma represents differentiation with respect to coordinates X_i. Substituting Eq. (4) into Eq. (3) and considering only uniform deformation (no torsion), the stress and thermal conductivity tensors due to the initial stress are all constant, i.e. $k_{ij,l} = \tau_{ij,l} = 0$ and the second term in Eq. (3) can be represented as:

$$\nabla\cdot(\mathbf{k}\cdot\nabla T) = \left(k_{ij}J_{jl}T_{,l}\right)_{,i} = (2-\delta_{ij})k_{lm}J_{il}J_{jm}T_{,ij} \tag{5}$$

in which δ_{ij} is the Kronecker delta ($=1$ when $i=j$, and 0 otherwise); J_{ij} is the Jacobi matrix defined in terms of the initial infinitesimal strain tensor ε_{ij}:

$$J_{ij} = \delta_{ij} + \frac{\partial u_i}{\partial x_j} = \delta_{ij} + \varepsilon_{ij} \tag{6}$$

Eqs. (3)–(6) fully describe the thermal conduction behavior of infinitesimally deformed solids.

3.3. One-dimensional thermo-mechanical wave problem

For an expanded laser beam completely illuminating the solid surface, a one dimensional model can be used in the analysis. For opaque metallic materials, the heat source due to a harmonically modulated laser radiation incident on the solid surface can be regarded as a surface source [18]. Then, Eq. (3) becomes:

$$\rho C i\omega T - (1+\varepsilon)^2 k(\tau)\frac{\partial^2 T}{\partial z^2} = \beta I_0 \delta(z) \tag{7}$$

with deformed state depth coordinate z. ω is the modulation angular frequency $\omega = 2\pi f$, β is the optical-to-thermal energy conversion efficiency, ε is the strain, I_0 is the laser intensity and $\delta(z)$ is the Dirac delta function. τ is the stress. This modified equation indicates a static stress dependent thermal conductivity along the z direction. For a sample of thickness L, the temperature at the front solid-air interface $z = 0$ is [19]:

$$T(0,f) = \frac{\beta I_0}{k(\tau)\sigma}\left[\frac{1+e^{-2\sigma L}}{1-e^{-2\sigma L}}\right]$$
$$\sigma = \sqrt{2i\pi f/\alpha(\tau)},\ \alpha(\tau) = k(\tau)/\rho C \tag{8}$$

Here σ is the complex thermal wavenumber and $\alpha(\tau)$ is the stress-dependent thermal diffusivity. Eq. (8) is valid under adiabatic (zero-heat-flux) boundary conditions at the solid–gas

interface which is reasonable for an aluminum alloy sample [18–21]. The actual complex PTMR signal $S(f)$ is related to the thermal-wave field by [19]:

$$S(f) = Y(f)T(f) \tag{9}$$

Here $Y(f)$ is the instrumental transfer function. The signal can be expressed in terms of amplitude and phase by:

$$\text{Amplitude: } A(f) \sim \|Y(f)\| I_0(f) \left(\frac{1}{e_m\sqrt{f}}\right) \frac{\left[(1-e^{-2\gamma})^2 + 4e^{-2\gamma}\sin^2\gamma\right]^{1/2}}{(1-e^{-\gamma}\cos\gamma)^2 + e^{-2\gamma}\sin^2\gamma} \tag{10a}$$

$$\text{Phase: } \Phi(f) = \arctan\left(\frac{-2e^{-\gamma}\sin\gamma}{1-e^{-2\gamma}}\right) - \frac{\pi}{4} + \Phi_0(f) \tag{10b}$$

where $e_m(\tau) = \sqrt{k(\tau)\rho C}$ is the solid effusivity, $\gamma \equiv 2\sqrt{\pi f}\kappa(\tau)$ and $\kappa(\tau) \equiv L/\sqrt{\alpha(\tau)}$. Both e_m and κ are functions of the thermal conductivity and other thermophysical parameters of the solid. $\Phi_0(f) = \arg[Y(f)]$ is the additional phase shift due to the instrumental transfer function $Y(f)$. It can be seen from Eq. (10b) that the PTMR phase only depends on the parameter γ which makes it suitable for the determination of κ from best fits of the theory to the experimental frequency-scan data.

4. Results and discussion

4.1. Elastic loading

The PTMR frequency-scanned signals under various stress conditions within the elastic regime are shown in Fig. 4(a). Both amplitude and phase signals are normalized with a convenient reference signal: that of the same sample under load-free conditions. The signals from the loading process (LP) and the relaxing (unloading) process (ULP) were recorded during each experiment. Fig. 4(b) shows the fixed-frequency PTMR amplitude and phase from several high-resolution LP and ULP stress scans (SS) of the sample within the elastic regime. These results exhibit good reproducibility and reversibility of the stress-dependent PTMR signal and demonstrate the connection between thermal properties and the stress–strain state of the sample. As the phase signal is completely determined by the parameter κ, it is clear that its changes are dominated by the thermal diffusivity, given that the

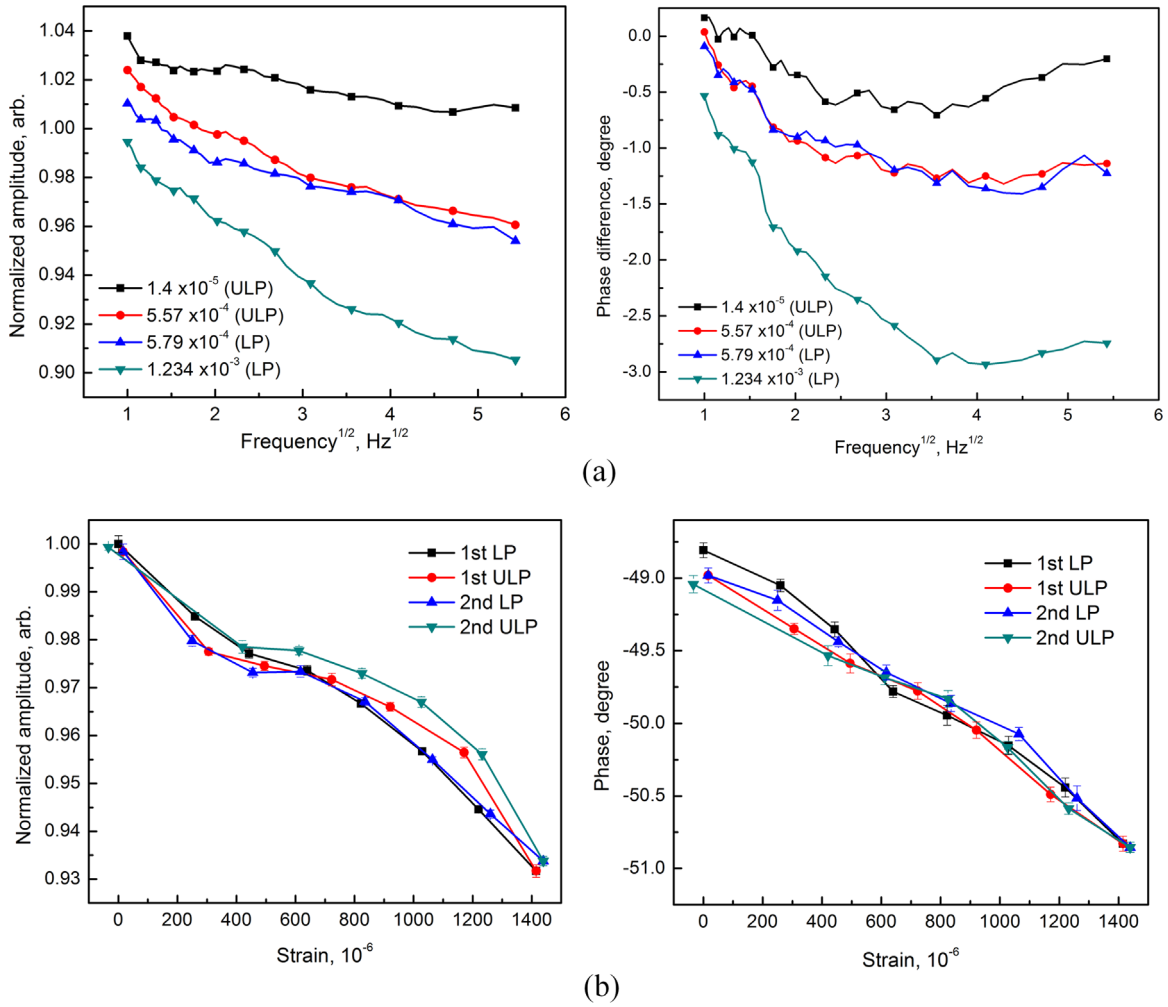

Fig. 4. Recorded PTMR signal from (a) frequency scans (FS) under various stress–strain conditions; (b) stress scans (SS) at 2.5 Hz (LP: loading process, ULP: unloading process).

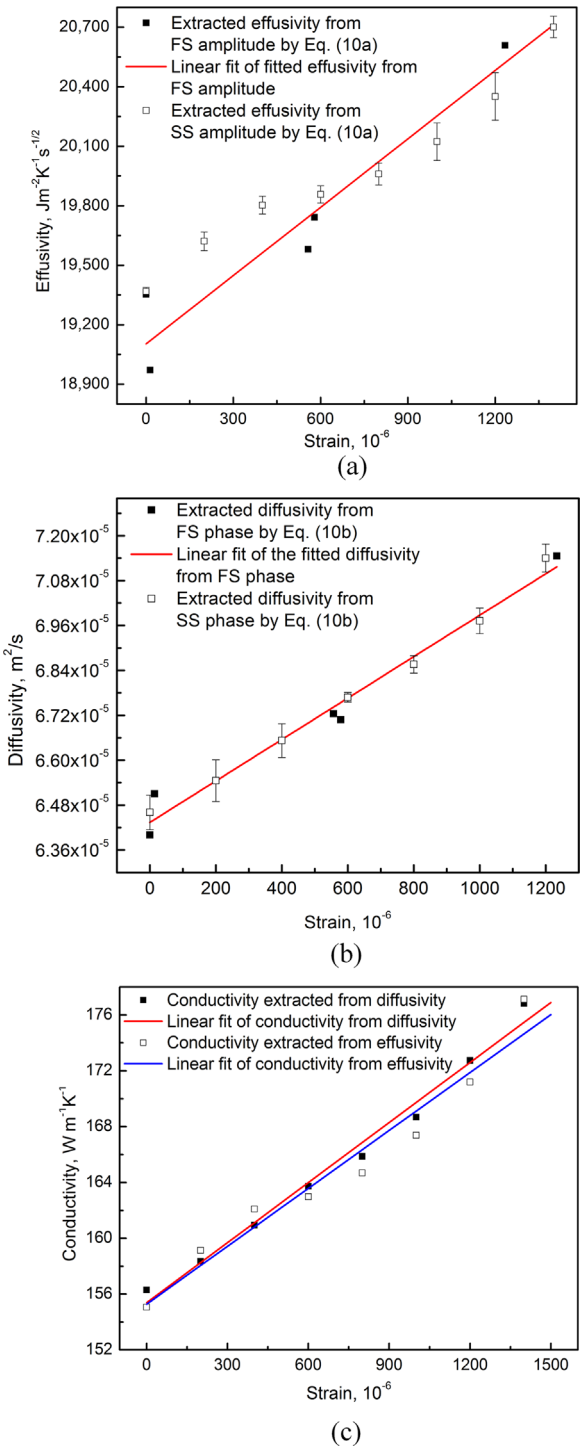

Fig. 5. Best fitted parameters from the experiments: (a) thermal effusivity from the amplitude; (b) thermal diffusivity from the phase; and (c) extracted thermal conductivity from both the effusivity and diffusivity values acquired from stress scans in (a) and (b).

sample thickness remains essentially constant within the elastic regime (thickness change is very much smaller than the thermal diffusion length at 2.5 Hz). The stress dependent diffusivity was extracted from fitting the phase data to Eq. (10b). Subsequently, by eliminating the influence of γ, the effusivity was also measured by fitting the amplitude data to Eq. (10a). Fig. 5 shows the quantitative results from fitting the frequency scan (FS) and stress scan (SS) data to the theory. The fitted effusivities and diffusivities from the FS tests show good agreement with those extracted from the SS tests and, as expected, the phase channel exhibits better measurement reliability than the amplitude because it is not sensitive to surface conditions or laser power. Furthermore, the linearly increasing patterns of both stress-dependent effusivity and diffusivity suggest a linear dependence of the thermal conductivity on stress, which is quantitatively verified in Fig. 5(c).

4.2. Plastic loading

The foregoing measurements performed within the sample's elastic regime suggest that thermal conductivity changes are solely responsible for, or the dominant cause of, the dependence of the PTMR signal on the state of stress, and the unstressed conductivity value can be recovered when the external load is removed. However, for tensile stressing that exceeds the elastic limit, plastic deformation will result in a permanent change of material properties. Based on the photo-thermo-mechanical methodology discussed above, the complete tensile loading stress–strain history can be investigated and mapped in terms of thermal property changes. For large deformations, the thermal-geometric parameter κ is uniquely measured from phase and it is a function of strain as shown in Fig. 6(a) and (b). The mechanical test consisted of three parts: elastic loading and unloading; plastic loading and unloading; and plastic reloading until fracture. The results show three distinct regimes, i.e. the elastic range, the strain hardening range, and the necking range. It is worth noting that these measurements were possible through PTMR even though the strain gauge failed after the real strain exceeded its detectable range. This is a significant feature of PTMR: it can assume the role of a non-contact "strain gauge" within and far beyond the operational range of commercial strain gauges. A "permanent set" (defined as the permanent change of the material shape after removal of stress occurring as the result of plastic deformation) was recorded from plastic unloading. The existence of maximum κ as shown in Fig. 6 (a) indicates the location on the strain axis (no independent values were available after the collapse of the strain gauge) of the ultimate strength of the material. Fig. 6(c) gives a typical qualitative example of the stress–strain relation of the aluminum alloy [22]. The strain dependent κ in Fig. 6(b) shows excellent analogy to the "stress" counterpart of the conventional stress–strain relation derived from tensile machines with respect to many features such as ultimate strength and the three distinct regions of mechanical performance.

5. Conclusions

A quantitative photo-thermo-mechanical investigation of the stress–strain relation in aerospace metal components was reported using frequency-domain PTMR detection. An aluminum sample typical of aircraft components was subjected to tensile stress in a home-made mechanical tensile tester equipped with a PTR setup. A one-dimensional thermo-mechanical-wave model was applied to determine the strain-dependent thermal diffusivity and effusivity from best-fitting the experimental phases and amplitudes. The results validated the existence of strain- (and thus, stress-) dependent thermal conductivity in the material and established a quantitative stress – PTR signal relation within the elastic regime. An excellent analogy was found with the conventional stress–strain relation within the elastic regime, while the PTMR parameter $\kappa(\tau) \equiv L/\sqrt{\alpha(\tau)}$ was shown to act as a virtual non-contact strain gauge across the entire range of applied stress from the stress-free state to fracture.

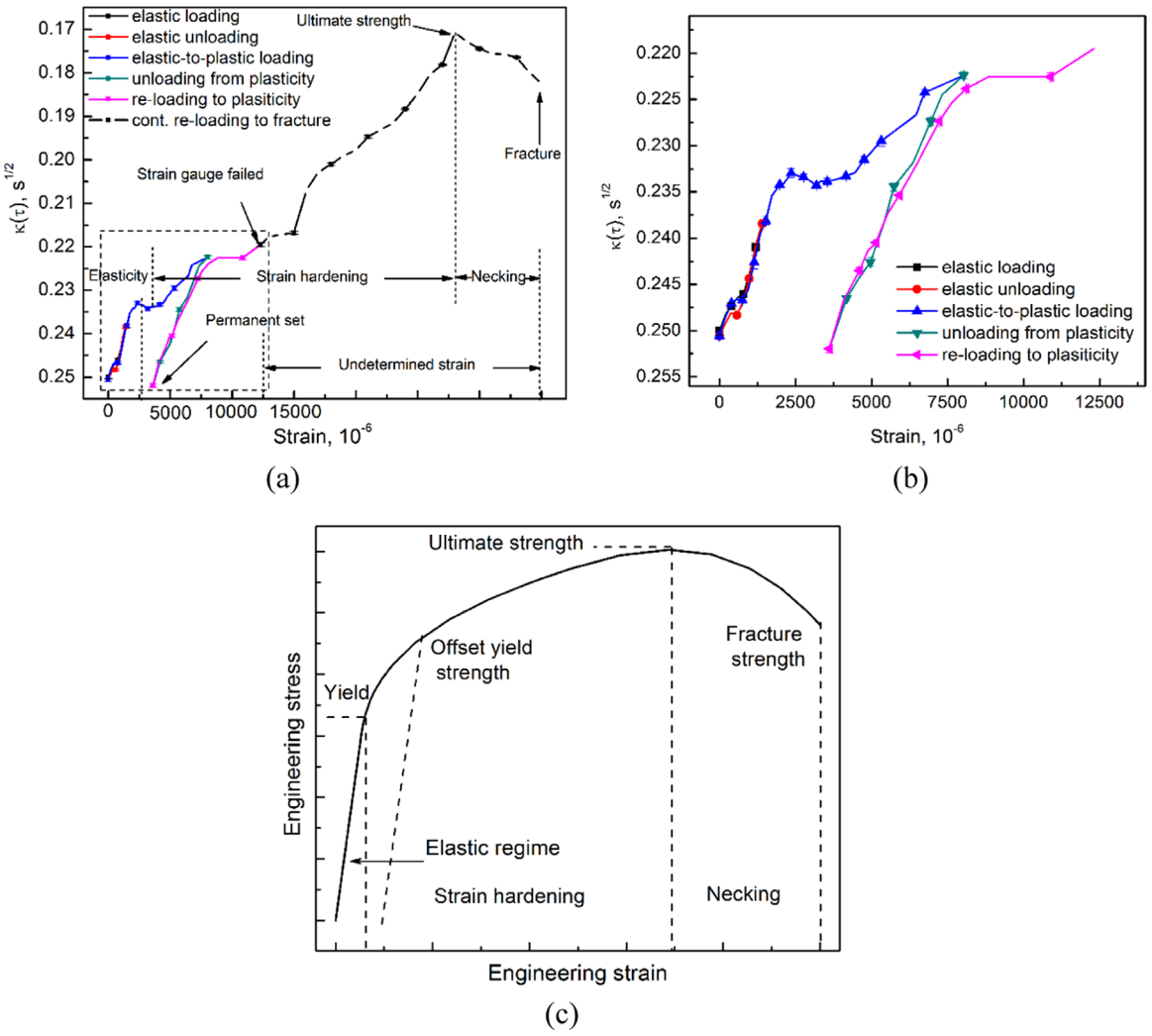

Fig. 6. (a) Full history of tensile loading up to fracture, represented quantitatively through the material parameter κ; (b) the right graph is the enlargement of the box shown in (a) with the vertical coordinate reversed to emphasize the analogy with the stress–strain relation as shown in (c) (Redrawn from Fig. 41 in Ref. [22]).

Acknowledgements

The authors are grateful to the Natural Sciences and Engineering Research Council of Canada (NSERC) for a Discovery grant to AM, and the Canada Research Chairs program. AM gratefully acknowledges the Chinese Recruitment Program of Global Experts (Thousand Talents). He also acknowledges the Foundation for Innovative Research Groups of the National Natural Science Foundation of China (Grant No. 61421002). HH gratefully acknowledges the China Scholarship Council (CSC) program (No. 201406070045). The authors are grateful to the University of Toronto Capstone project team (Q. Cao, F. Chang, L. S. Mu, L. Tian, 2016) for the much improved mechanical tensile rig re-design.

References

[1] Crecraft DI. The measurement of applied and residual stresses in metals using ultrasonic waves. J Sound Vib 1967;5:173–92.
[2] Hsu NN. Acoustical birefringence and the use of ultrasonic waves for experimental stress analysis. Exp Mech 1974;14:169–76.
[3] Gogotsi Y, Baek C, Kirscht F. Raman microspectroscopy study of processing-induced phase transformations and residual stress in silicon. Semicond Sci Technol 1999;14:936–44.
[4] M. Moore, W. Evans, Mathematical correction for stress in removed layers in X-ray diffraction residual stress analysis, SAE Technical Paper 1958; DOI: 10.4271/580035, No. 580035.
[5] Landau LD, Lifshitz EM. Theory of elasticity, 119–122. Bristol: Pergamon Press; 1959. p. 15–7.
[6] Biot MA. The influence of initial stress on elastic waves. J Appl Phys 1940;11:522–30.
[7] Hughes DS, Kelly JL. Second-order elastic deformation of solids. Phys Rev 1953;92:1145–9.
[8] Rose JL. Ultrasonic waves in solid media. New York: Cambridge University Press; 1999. p. 299–306.
[9] Wong AK, Jones R, Sparrow JG. Thermoelastic constant or thermoelastic parameter? J Phys Chem Solids 1987;48:749–53.
[10] Kasai M, Sawada T. Photoacoustic and photothermal phenomena, II. In: Murphy JC, Maclachlan Spicer JW, Aamodt LC, Royce BSH, editors. . Berlin: Springer-Verlag; 1990. p. 33–6.
[11] Muratikov KL, Glazov AL, Rose DN, Dumar JE. Photoacoustic effect in stressed elastic solids. J Appl Phys 2000;88:2948–55.
[12] Muratikov KL. Theory of stress influence on the photoacoustic thermoelastic signal near the vertical crack tips. Rev Sci Instrum 2003;74:722–4.
[13] Munidasa M, Mandelis A, Ball M. Buried thermoplastic layer diagnostics by the use of combined frequency-domain and impulse response photo-thermo-mechanical radiometry. Rev Sci Instrum 1998;69:507–11.
[14] Cao Q, Chang F, Mu LS, Tian L. Capstone project: photothermal radiometry NDT design Toronto: University of Toronto; 2016 (unpublished).
[15] Achenbach JD. Wave propagation in elastic solids. New York: North-Holland Publishing; 1973. p. 46–59.
[16] ASTM B308/B308M-10 standard specification for aluminum-alloy 6061-T6 standard structural profiles, ASTM International, West Conshohocken, PA; 2010. http://dx.doi.org/10.1520/B0308_B0308M-10.

[17] Qian M. New thermoelastic technique for detection of residual stress distribution in solids. Chin J Acoust 1995;14:98–106.
[18] Rose L. Point-source representation for laser-generated ultrasound. J Acoust Soc Am 1984;75:723–32.
[19] Balderas-López JA, Mandelis A. Self-normalized photothermal technique for accurate thermal diffusivity measurements in thick metal layers. Rev Sci Instrum 2003;74:5219–25.
[20] Mandelis A. Diffusion-wave fields: mathematical methods and green functions. New York: Springer; 2001. p. 100–24.
[21] Garcia JA, Mandelis A, Farahbakhsh B, Lebowitz C, Harris I. Thermophysical properties of thermal sprayed coatings on carbon steel substrates by photothermal radiometry. Int J Thermophys 1999;20:1587–602.
[22] MacKenzie DS. In: Totten GE, MacKenzie DS, editors. Handbook of aluminum: volume 2: alloy production and materials manufacturing. Abingdon: Taylor & Francis Group; 2003. p. 396.